ELSEVIER

Earth and Planetary Science Letters 160 (1998) 537–550

EPSL

Low-degree partial melting trends recorded in upper mantle minerals

Pierre Schiano [a,*], Bernard Bourdon [a], Robert Clocchiatti [b], Dominique Massare [b], Maria E. Varela [b], Yan Bottinga [a]

[a] *Laboratoire de Géochimie–Cosmochimie (CNRS–URA 1758), IPG Paris et UFR Sciences de la Terre, Université Paris VII, 4 place Jussieu, 75252 Paris cedex 05, France*

[b] *Laboratoire Pierre Süe, CEA–CNRS–UMR 9956, Centre d'Etude Nucléaire de Saclay, 91191 Gif-sur-Yvette, France*

Received 1 October 1997; revised version received 9 March 1998; accepted 1 April 1998

Abstract

The study of glass inclusions inside mantle minerals provides direct information about the chemistry of naturally occurring mantle-derived melts and the fine-scale complexity of the melting process responsible for their genesis. Minerals in a spinel lherzolite nodule from Grande Comore island contain glass inclusions which, after homogenization by heating, exhibit a continuous suite of chemical compositions clearly distinct from that of the host basanitic lava. The compositions range from silicic, with nepheline–olivine normative, 64 wt% SiO_2 and 11 wt% alkali oxides, to almost basaltic, with quartz normative, 50 wt% SiO_2 and 1–2 wt% alkali oxides. Within a single mineral phase, olivine, the inferred primary melt composition varies from 54 to 64 wt% SiO_2 for MgO content ranging from 8 to 0.8 wt%. An experimental study of the glass and fluid inclusions indicates that trapped melts represent liquids that are in equilibrium with their host phases at moderate temperature and pressure ($T \approx 1230$ºC and $P \approx 1.0$ Gpa for melts trapped in olivine). Quantitative modelling of the compositional trends defined in the suite shows that all of the glasses are part of a cogenetic set of melts formed by fractional melting of spinel lherzolite, with F varying between 0.2 and 5%. The initial highly silicic, alkali-rich melts preserved in Mg-rich olivine become richer in FeO, MgO, CaO and Cr_2O_3 and poorer in SiO_2, K_2O, Na_2O, Al_2O_3 and Cl with increasing melt fractions, evolving toward the basaltic melts found in clinopyroxene. These results confirm the connection between glass inclusions inside mantle minerals and partial mantle melts, and indicate that primary melts with SiO_2 >60 wt%, alkali oxides >11%, FeO <1 wt% and MgO <1 wt% are generated during incipient melting of spinel peridotite. The composition of the primary melts is inferred to be dependent on pressure, and to reflect both the speciation of dissolved CO_2 and the effect of alkali oxides on the silica activity coefficient in the melt. At pressures around 1 GPa, low-degree melts are characterized by alkali and silica-rich compositions, with a limited effect of dissolved CO_2 and a decreased silica activity coefficient caused by the presence of alkali oxides, whereas at higher pressures alkali oxides form complexes with carbonates and, consequently, alkali-rich silica-poor melts will be generated.

Keywords: partial melting; glass; inclusions; spinel lherzolite

* Corresponding author. Tel.: +33 (1) 4427-4915; Fax: +33 (1) 4427-3752; E-mail: schiano@ipgp.jussieu.fr

0012-821X/98/$19.00
PII S0012-821X(98)00109-5

1. Introduction

Geochemical studies of mantle-derived magmas erupted at the Earth's surface have shown that one of the main factors controlling their chemistry is the degree of partial melting. However, geologists rarely have direct access to pristine mantle melts, and laboratory experimental partial melting of peridotite essentially documents the chemical composition of large melt fractions ($F \geq 10\%$) (e.g. [1–10]). Therefore, several aspects of melting models remain hypothetical. In particular, the major element composition of the lowest melt fractions from upper mantle peridotite is still a matter of debate [11–13]. Baker et al. [14], using both the diamond-aggregate extraction technique and thermodynamic calculations, have reported the compositions of low-degree ($F = 2$ to 5%) melts of peridotite which extend to high SiO_2, Na_2O and low FeO and MgO contents at pressures around 1.0 GPa. These results confirm the high Na_2O and low FeO and MgO contents for near-solidus mantle melts calculated by Langmuir et al. [15], and the prediction of Kinzler and Grove [16] that the abundance of SiO_2 in melts from peridotites decreases as the extent of melting increases. However, they contradict earlier experiments that predicted low SiO_2 concentrations in melts produced by less than about 10% melting (e.g. [17]). An additional problem is to reconcile these results with natural data on volcanic rocks in oceanic islands [18], that are thought to be derived from a low extent of melting and typically have undersaturated compositions (basanites or nephelinites) with low SiO_2, and high FeO and Na_2O abundance (e.g. [19–21]).

In the present study, the approach was to identify and examine directly near-solidus mantle melts preserved as quenched glass inclusions in minerals in upper mantle xenoliths. We have not considered interstitial glass samples found in xenoliths because they appear to be open systems and are prone to chemical modification during ascent of the host xenolith (e.g. Refs. [22,23]), whereas melt/fluid inclusions inside minerals behave as closed and nearly isochoric systems. Previous studies of glass inclusions in peridotite xenoliths have shown that high-silica glasses are a common feature of spinel lherzolite minerals [24,25], and a general link between these silica-rich inclusions and the character of near-solidus partial melts of peridotite has been suggested [14,25–27]. The new contribution of this study is the documentation of a series of glass inclusions whose wide compositional range, from silicic to almost basaltic compositions, can be quantitatively modelled by near-solidus melting of a mildly depleted peridotite. This continuous series of inclusion compositions in a spinel peridotite sample and the compositional trends recorded in this suite confirm the connection between silica-rich melt inclusions and the compositions of partial melts. Furthermore, the results extend previous studies arguing in favour of silica-rich melts at low degree of melting, in establishing that near-solidus primary melts of peridotite could have SiO_2 contents of >60 wt% for MgO contents <1 wt%.

2. Xenolith and glass inclusion description

The xenolith we studied (CLG1) was found in silica-undersaturated, basanitic lavas from La Grille volcano, on Grande Comore island in the western Indian Ocean. According to its modal composition, it can be classified as anhydrous spinel lherzolite (Table 1). The main phase is olivine (ol), which occurs as porphyroclasts ($Fo_{90–92}$) with undulatory extinction, and as strain-free euhedral neoblasts ($Fo_{86–87}$) forming equigranular domains. Orthopyroxene (opx) porphyroclasts ($En_{87–89}$) show exsolution lamellae of clinopyroxene (cpx), mostly restricted to the core of the crystals. Spinel (sp) (27–43 wt% Cr_2O_3) occurs both as vermicular grains and as rounded interstitial porphyroclasts. Recrystallized clinopyroxene ($Wo_{37–47}$, $En_{46–57}$) is present as interstitial neoblasts.

The CLG1 xenolith contains abundant glass inclusions (size <100 μm) in the porphyroclasts and the neoblasts. They occur as trails of rounded secondary inclusions along fractures in olivine and orthopyroxene porphyroclasts. In contrast, inclusions in clinopyroxene neoblasts are primary, their distribution is random and their shape is controlled by the crystallographic structure and the growth of the host mineral. Secondary CO_2 fluid inclusions containing coexisting vapour and liquid phases are observed in porphyroclasts. Their association with glass inclusions, and the existence of multiphase inclusions consisting of silicate glass and CO_2-rich fluid, sug-

Table 1
Representative analyses (wt%) of mineral phases in CLG1 xenolith

	ol (N)	ol (N)	ol (P)	ol (P)	opx	opx	cpx	cpx	sp (V)	sp (I)	sp (In)
SiO_2	39.82	40.22	40.10	40.60	55.47	55.08	52.41	53.24	0.09	0.10	0.05
Al_2O_3	0.00	0.00	0.02	0.03	3.16	3.51	3.76	2.67	26.29	24.46	37.35
TiO_2	0.02	0.03	0.02	0.00	0.04	0.04	0.40	0.32	0.22	1.21	0.10
MnO	0.22	0.23	0.12	0.12	0.18	0.16	0.12	0.12	0.19	0.21	0.18
FeO	13.23	12.29	9.62	9.72	5.94	6.24	4.57	3.55	13.99	22.98	14.63
MgO	46.80	47.04	50.02	49.40	33.24	33.30	16.94	18.42	16.09	14.15	17.54
CaO	0.28	0.37	0.09	0.09	1.29	1.15	20.22	19.35	0.03	0.04	0.00
K_2O	0.00	0.00	0.00	0.00	0.00	0.00	0.00	0.00	0.01	0.00	0.00
Na_2O	0.00	0.00	0.00	0.00	0.08	0.07	0.72	0.66	0.00	0.01	0.00
NiO	0.23	0.29	0.42	0.33	0.07	0.09	0.07	0.05	0.18	0.22	0.32
Cr_2O_3	0.03	0.06	0.00	0.00	0.82	0.72	1.25	1.69	43.05	36.83	30.20
	100.63	100.53	100.41	100.29	100.29	100.36	100.46	100.07	100.14	100.21	100.37
Mg#	0.86	0.87	0.90	0.90	0.91	0.91	0.87	0.90			

Compositions were measured with a CAMECA SX 50 electron microprobe (Camparis, Paris), using an accelerating voltage of 15 kV, sample current of 40 nA and a focussed beam.
ol (N), olivine neoblast; ol (P), olivine porphyroclast; opx, orthopyroxene; cpx, clinopyroxene; sp (V), vermicular spinel; sp (I), interstitial spinel; sp (In), spinel included in olivine; Mg#, molar Mg/(Mg + Fe), all Fe as FeO.

gest that both glass and fluid inclusions have been trapped from an immiscible mixture of silicate melt and CO_2 fluid. Some melt inclusions contain both glass and 'daughter' minerals, mainly orthopyroxene ($En_{86–89}$) and clinopyroxene (Table 2), grown by closed-system crystallization of the trapped melt. These 'daughter' clinopyroxenes display a large compositional range, from $Wo_{35–39}En_{54–57}$ in inclusions inside porphyroclasts to $Wo_{43–48}En_{44–48}$ in inclusions inside vermicular spinel.

The minimum *P–T* conditions of the silicate melt trapped inside the inclusions were estimated from an experimental study of the inclusions. An estimate of the liquidus temperature of the melt is given by T_m, the final melting temperature of the enclosed 'daughter' minerals [28,29]. As mantle minerals are relatively incompressible, inclusions behave as isochoric systems during experiments [28,30], and T_m is equal to the liquidus temperature of the melt at the pressure of trapping. Heating experiments performed with a high-temperature optical apparatus [31] on inclusions in olivine porphyroclasts give a final melting temperature for the enclosed 'daughter' minerals (opx and cpx) of 1230 ± 20°C. Complete homogenization of the inclusions could not be reached during the heating experiments, because of the persistence of CO_2 bubbles in the melt. Petrographical evidence for the simultaneous trapping of glass and

Table 2
Representative analyses (wt%) of 'daughter' mineral phases inside composite inclusions trapped in mineral phases from CLG1 xenolith

	opx (ol)	opx (ol)	cpx (ol)	cpx (sp)
SiO_2	56.55	56.46	53.83	46.68
Al_2O_3	1.08	1.80	1.70	9.47
TiO_2	0.05	0.13	0.29	2.24
MnO	0.13	0.24	0.24	0.15
FeO	7.25	6.17	6.58	4.12
MgO	34.09	32.99	19.49	14.25
CaO	0.78	1.87	17.78	21.21
K_2O	0.01	0.01	0.00	0.00
Na_2O	0.09	0.11	0.21	0.57
NiO	0.12	0.13	0.08	0.05
Cr_2O_3	0.20	0.56	0.24	0.89
	100.35	100.47	100.44	99.63
Mg#	0.89	0.91	0.84	0.86

Compositions were measured with a CAMECA SX 50 electron microprobe (Camparis, Paris), using an accelerating voltage of 15 kV, sample current of 40 nA and a focussed beam.
opx (ol), orthopyroxene inside composite inclusions in olivine porphyroclasts; cpx (ol), clinopyroxene inside composite inclusions in olivine porphyroclast; cpx (sp), clinopyroxene inside composite inclusions in vermicular spinel; Mg#, molar Mg/(Mg + Fe), all Fe as FeO.

CO_2 inclusions can be used to derive a melt entrapment pressure, using the liquidus temperature (1230°C) obtained from melt inclusions along with

P–V–T data on associated CO_2 fluid inclusions. The observed maximum density for the CO_2 inclusions, obtained using the homogenization method based on the CO_2 vapour–liquid equilibrium [28], is 0.97 g cm^{-3}. This value corresponds to a temperature of −8ºC at which liquid and gaseous CO_2 homogenize, obtained during microthermometry experiments. It implies a minimum trapping pressure for the associated glass inclusions of 0.9 GPa at 1230ºC. This pressure value is a minimum estimate, because it is unlikely that the fluid inclusions have been closed systems since their formation. Decrepitation of some CO_2-fluid inclusions are telltale signs of partial escape of the original gas.

The composition of the melts trapped in the inclusions was determined on homogeneous, quenched glasses obtained after heating the inclusions up to the liquidus temperature to melt any 'daughter' minerals. Comparison of these rehomogenized inclusions with unheated glassy inclusions exempt of 'daughter' minerals, can be used to estimate the effect of post-entrapment processes such as crystallization at the inclusion walls, since these processes ought to be reversible in homogenization experiments. In olivine porphyroclasts, the similarity of compositions for rehomogenized inclusions and unheated glassy inclusions indicates that no significant post-entrapment change has taken place. This absence of reaction between secondary glass inclusions and their host olivine crystals is in agreement with the absence of chemical zonation at the olivine/inclusion interface as shown by electron microprobe traverses. In contrast, the majority of primary inclusions in clinopyroxene have experienced post-entrapment evolution, indicated by high levels of crystallization at the inclusion walls.

The major element compositions of the inclusions, after homogenization by heating, show a continuous evolution from high-SiO_2 melts inside olivine porphyroclasts to low-SiO_2 melts inside clinopyroxene neoblasts (Table 3). The former contain high contents of SiO_2 ($\geq$60 wt%), Al_2O_3 ($\geq$20 wt%), alkali oxides (Na_2O $\geq$6 wt% and K_2O $\geq$4 wt%) and low contents of MgO ($\leq$2 wt%), FeO ($\leq$2 wt%) and CaO ($\leq$5 wt%). It should be noted that, despite a high silica content, glass inclusions in olivine are characterized by normative olivine and nepheline. They also have high chlorine levels ($\geq$3500 ppm), but their H_2O concentrations are low ($\leq$0.02 wt%, based on FTIR spectroscopy analyses of three inclusions). The persistence of CO_2 bubbles in the melt during the heating experiments indicates oversaturation of glass inclusions with CO_2. These features are typical of glass inclusions inside mantle minerals, and have been interpreted as indicative of a metasomatic melt phase [24]. On the other hand, low-SiO_2 glass inclusions in recrystallized clinopyroxene have compositions ranging from alkali basalts to quartz tholeiites. They contain 51–55 wt% SiO_2, 14–17 wt% Al_2O_3, 10–15 wt% CaO, $\leq$0.5 wt% TiO_2, 10–13 wt% MgO, 3–6 wt% FeO, $\leq$4 wt% Na_2O wt%, $\leq$1 wt% K_2O and $\leq$500 ppm Cl.

3. Equilibrium between silicic melts and ultramafic assemblages

Whether high-SiO_2 melt inclusions are in equilibrium with Mg-rich mantle phase is an important point of debate. Disequilibrium melt compositions, which can result from decompression melting of a xenolith during its transport to the surface, would lead to crystal–melt reaction. By contrast, the glass phase inside inclusions in olivine porphyroclasts is homogeneous, and there are no indications that the trapped melt reacted with the host phase. This strongly suggests the attainment of equilibrium between trapped high-SiO_2 melts and their host olivine crystals. High-pressure liquidus experiments on highly silicic melts performed by Draper and Green [26] indicate that, under anhydrous conditions and when saturated with COH fluid, melts with compositions comparable to the glass inclusions are saturated with harzburgitic minerals (ol and opx) as liquidus phases. The observed high Mg numbers (Mg#, defined as molar $Mg/(Mg + Fe^{2+})$, with all Fe as FeO), between 0.89 and 0.91, of the 'daughter' orthopyroxene crystallized from the silicic melts trapped in olivine porphyroclasts (Table 2) support the experimental results. An additional constraint on the composition of melts in equilibrium with lherzolite or harzburgite residual mineralogy has been recently given by Falloon et al. [13]. These authors have shown that silicic melts in equilibrium with olivine of Mg# = 0.90 would have olivine–nepheline normative compositions, which is

Table 3
Selected representative analyses (wt%) of glass inclusions (gl), after homogenization by heating and quenching, and host minerals from CLG1 xenolith

	gl	ol	gl	ol	gl	ol	gl	opx	gl	opx	gl	opx	gl	cpx	gl	cpx	gl	cpx
SiO_2 wt%	63.25	40.61	60.71	40.76	54.60	40.20	56.25	55.90	54.39	56.49	55.42	55.93	53.65	53.05	51.70	53.21	52.24	52.29
TiO_2	0.34	0.04	0.21	0.00	0.55	0.07	0.60	0.10	0.96	0.05	0.67	0.00	0.23	0.09	0.35	0.12	0.29	0.08
Al_2O_3	20.06	0.04	17.59	0.03	17.19	0.01	15.91	2.66	15.15	2.12	15.48	2.73	15.72	4.25	15.37	3.51	14.47	3.64
FeO	1.08	10.07	3.32	9.40	4.55	9.19	4.70	5.93	5.26	6.10	5.30	5.57	5.56	2.71	4.50	3.41	4.90	2.84
MgO	0.83	49.46	4.50	49.89	8.05	50.17	9.17	33.00	10.45	32.83	9.58	33.10	9.64	16.96	10.80	18.65	11.01	17.53
CaO	3.00	0.14	2.52	0.09	6.79	0.13	5.75	1.91	6.56	2.04	7.94	1.78	11.11	19.85	14.88	18.26	11.96	20.44
Na_2O	7.35	0.00	5.71	0.00	5.36	0.00	4.71	0.12	4.89	0.10	4.06	0.12	1.85	0.95	0.94	0.83	1.96	0.70
K_2O	4.19	0.00	3.52	0.00	1.84	0.00	2.06	0.00	1.60	0.00	1.43	0.01	1.10	0.03	0.32	0.00	0.85	0.00
Cr_2O_3	0.03	0.00	0.01	0.00	0.04	0.00	0.15	0.81	0.13	0.94	0.08	0.98	0.37	1.25	0.58	1.11	0.91	1.24
Cl ppm	6620	0	4280	0	3000	0	1680	0	1570	0	1090	0	330	0	220	0	310	0
$K_D^{ol/liq}$	0.16		0.26		0.32													
Mg#	0.58	0.90	0.71	0.90	0.74	0.90	0.78	0.91	0.78	0.91	0.76	0.91	0.79	0.92	0.81	0.91	0.80	0.92
Normative composition																		
qz													1.2		1.5			
or	24.8		20.8		10.9		12.2		9.5		8.5		6.5		1.9		5.0	
ab	57.2		48.3		36.4		39.9		37.2		34.4		16.7		8.0		16.6	
an	9.4		12.0		17.4		16.2		14.7		19.8		31.3		36.8		28.2	
ne	2.7				4.9				2.3									
di	4.5		0.4		13.1		9.9		14.3		15.7		19.2		29.6		24.9	
hy			14.6				5.0				8.3		24.6		20.5		18.3	
ol	0.9		1.5		15.3		14.9		19.6		12.0						4.2	
il	0.7		0.4		1.0		1.1		1.8		1.3		0.4		0.7		0.6	

Glass compositions were measured with a CAMECA SX 50 electron microprobe (Camparis. Paris) using an accelerating voltage of 15 kV, sample current of 10 nA and a beam of 20 μm. $K_D^{ol/liq}$ is defined as $(X_{Fe}^{ol} X_{Mg}^{liq})/(X_{Mg}^{ol} X_{Fe}^{liq})$.
Normative composition: qz, quartz; or, orthoclase; ab, albite; an, anorthite; ne, nepheline; di, diopside; hy, hypersthene; ol, olivine; il, ilmenite.

in agreement with the composition of the inclusions inside olivine porphyroclasts reported in this study. Both lines of evidence clearly indicate that the silicic melts preserved as inclusions represent liquids in equilibrium with their host mantle olivine at upper mantle temperatures and pressures.

On the other hand, melts showing basaltic compositions occur as primary inclusions in recrystallized clinopyroxene, i.e. they are cogenetic with their host phases. These observations and the large range of chemical compositions in the glass inclusions suggest that the melts trapped in the xenolith are locally in equilibrium with their enclosing crystalline phases. As all the crystalline phases in the xenolith are not cogenetic, the range in melt compositions can be preserved. The various melts may interact but for kinetic reasons, in particular the large difference in viscosity between the partial melting products, they did not mingle significantly within the xenolith [32].

The Fe–Mg exchange coefficient ($K_D^{ol/liq} = (X_{Fe}^{ol} X_{Mg}^{liq})/(X_{Mg}^{ol} X_{Fe}^{liq})$) values obtained for the inclusions range between 0.33 and 0.16, which is much less than the 1 atm value of 0.30 ± 0.03 determined by Roeder and Emslie [33]. They also extend to even lower $K_D^{ol/liq}$ (with higher SiO_2) than previously reported in experimental near-solidus melting of mantle peridotite [14], and in high-pressure experiments on natural compositions [26,34]. Low $K_D^{ol/liq}$ values are generally considered to be related to the high alkali content of the melt [12,14,26], but could reflect experimental problems like quench crystallization [35].

It should be noted that evidence from fluid inclusions and heating experiment results suggest equilibration of the high-silica melts at 0.9 GPa and 1230ºC. This temperature is close to the peridotite solidus at this pressure [15], and this supports the hypothesis that the silicic melts represent near-solidus partial melts at moderate pressure. A melting pressure of 0.9 GPa indicates lithospheric conditions, as the oceanic lithosphere in the Comores is >100 Ma old and probably thicker than 80 km [36]. However, at this pressure, the near-solidus temperature reached by the xenolith is higher than the temperature for normal old oceanic lithosphere. A possible explanation is that the lithosphere may have been locally heated, probably by hotspot volcanism.

4. Compositional variations in low-degree melts

Although there is some scatter, the compositional variations in the rehomogenized inclusions inside olivine and pyroxene define a coherent trend on variation diagrams (Fig. 1). The observed correlations cannot be explained by a two-component mixing relationship, especially if one component is the host basanitic magma, because many of the trends in Fig. 1 are not linear and do not overlap with the basanite field (e.g., in the MgO, Na_2O versus SiO_2 diagrams). In this section, we discuss several models including crystal fractionation, mantle/melt reaction and progressive melting, that could potentially explain the observed trends. Although there is evidence for the importance of clinopyroxene crystallization, the partial melting model alone provides a straightforward explanation of the observed correlations.

Olivine, orthopyroxene and clinopyroxene are the only neoblastic phases present in the CLG1 nodule. The well-defined negative CaO–Na_2O correlation is not consistent with olivine–orthopyroxene fractionation. Conversely, substantial clinopyroxene fractionation would be expected to produce a negative correlation between CaO and Na_2O similar to that observed, and the primary character of the basaltic glass inclusions in clinopyroxene neoblasts clearly indicate that the trapped melts are saturated with clinopyroxene. Experimental evidence on tholeiitic compositions (e.g. [37]) indicates that clinopyroxene fractionation is only possible at a pressure that cannot be much lower than the pressure of melting, because in phase diagrams the clinopyroxene phase volume expands as the pressure increases. However, there are some aspects of the data which cannot be reconciled with clinopyroxene fractionation. Notably, such crystallization would progressively lower the MgO and increase the FeO contents of the melts, which is the inverse of what is observed. Finally, as illustrated in Fig. 2, progressive cpx + ol (or opx) extraction from an initial melt composition similar to the basaltic glass inclusions cannot produce the composition of the most silicic glass inclusions, even if clinopyroxene crystallization may cause some of the observed scatter within the trends.

Open-system processes, involving melt–peridotite exchange, can be considered as plausible mechanisms for the origin of SiO_2-rich glass inclusions

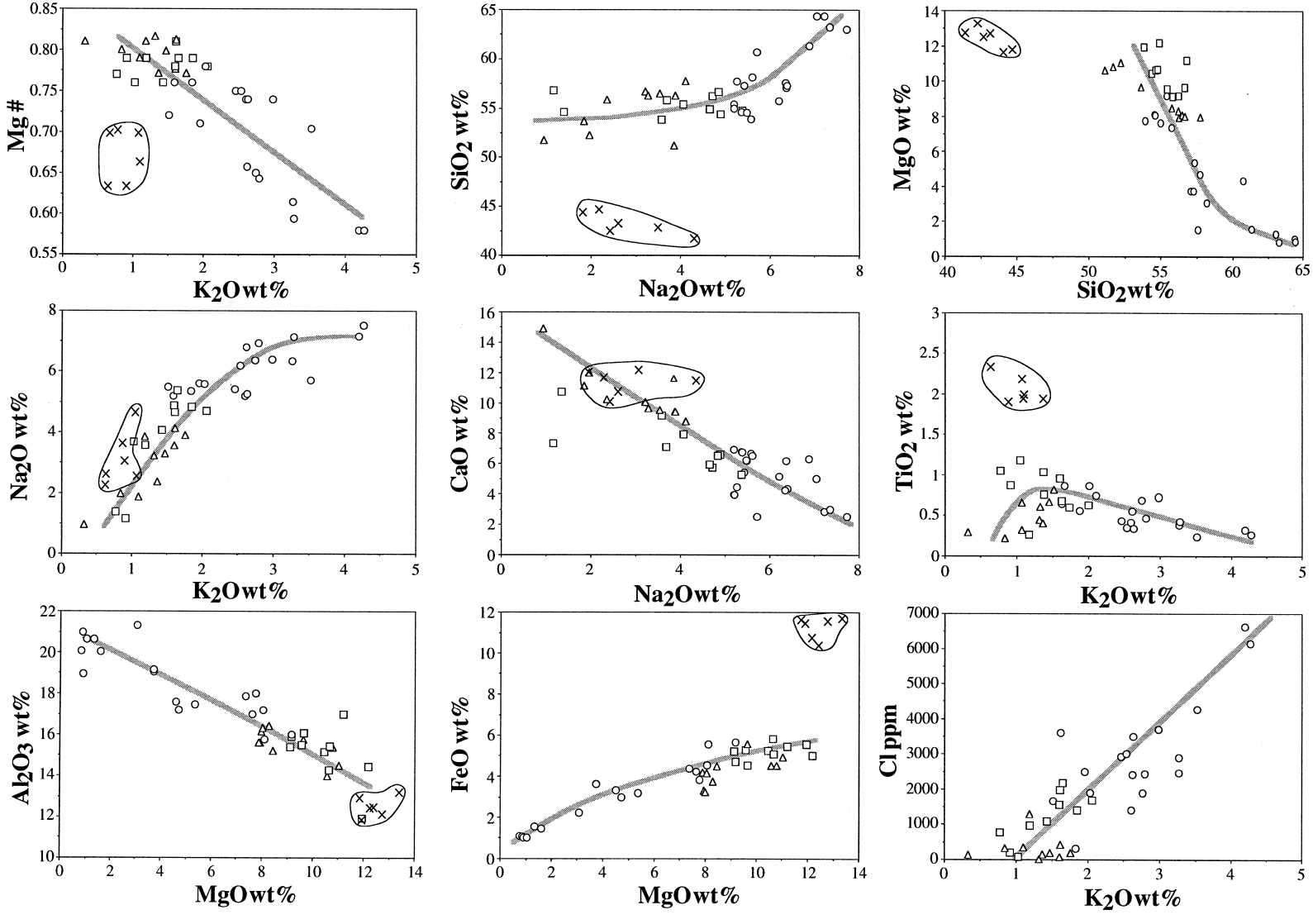

Fig. 1. Representative major element variation diagrams for glass inclusions trapped in olivine (circles), orthopyroxene (squares) and clinopyroxene (triangles) from CLG1 xenolith, after homogenization by heating experiments. Major element composition for La Grille host basanites [63,64] (crosses) are added for comparison. Mg# is defined as molar $Mg/(Mg + Fe^{2+})$, all Fe as FeO.

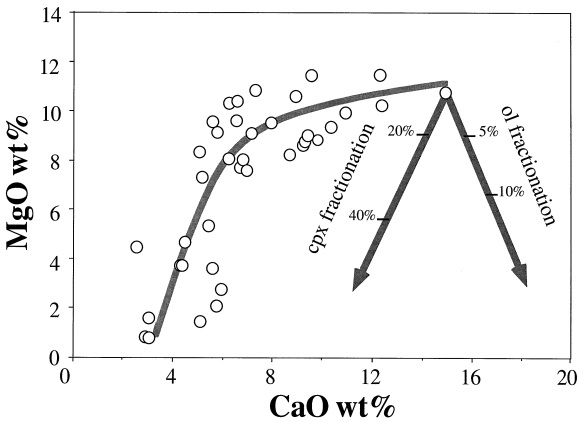

Fig. 2. Plot of MgO wt% against CaO wt% for glass inclusions trapped in olivine, orthopyroxene and clinopyroxene, after homogenization by heating experiments. Arrows show the effect of fractional crystallization of clinopyroxene (*cpx*) and olivine (*ol*) from an initial melt composition similar to the basaltic glass inclusions. Olivine Fo_{90} and clinopyroxene $Wo_{38}En_{56}$ were used for the calculations. Obviously, clinopyroxene–olivine (or orthopyroxene) fractionation cannot account for the chemical variations of the melts trapped as inclusions (see text for further discussion).

(e.g. [27,38]). Kelemen and co-authors [39,40] have shown that percolating basaltic melts, in order to remain on the ol + opx + cpx cotectics, may react during their ascent with mantle peridotite by dissolving pyroxenes (cpx + opx) and crystallizing olivine. Since more orthopyroxene is dissolved than clinopyroxene, the resulting melts will be characterized by SiO_2-enriched compositions [39,40]. However, such an open-system process, which has to occur over a large range of pressure, would probably not preserve the large compositional range observed on a cm-scale. Furthermore, a melt–peridotite interaction process would imply that the most evolved melts are silica-rich while the earlier melts are more akin to basalts. This is in contradiction with petrological observations which suggest that the basaltic melts which are found in late-formed clinopyroxene neoblasts were the last melts to be generated, whilst the silicic melts are found in primary Mg-rich olivines.

The chemical trends recorded by the inclusions can be the result of progressive melting, producing initially highly silicic, alkali-rich melts trapped in magnesian olivine. With progressively increasing melt fractions, the melts become richer in FeO, MgO, CaO and Cr_2O_3 and poorer in SiO_2, K_2O, Na_2O, Al_2O_3 and Cl, evolving toward the basaltic compositions found in recrystallized clinopyroxene. The Mg# in the glasses varies from 0.57 to 0.82 over this inferred melting interval. A comparison of these results with the diamond-aggregate melting experiments on peridotite performed by Baker et al. [14] shows some analogies. Both the experiments and the inclusion data show that at 1 GPa, near-solidus melts are enriched in SiO_2, Al_2O_3, and Na_2O, and depleted in FeO, MgO and CaO relative to higher-degree melts. In particular, they display a positive correlation between MgO and FeO together with an increase in Mg#, a result also predicted by Kinzler and Grove [16] for low degrees of melting. Moreover, TiO_2 displays a complex behaviour in both experimental melts and glass inclusions, first increasing then decreasing with degree of melting (Fig. 1). This anomalously low abundance of TiO_2 for the lowest degrees of melting reflects higher $D_{Ti}^{cpx/liq}$, related to changes in the pyroxene composition during early stages of melting [14].

However, there are some marked differences between the glass inclusion data and the diamond-aggregate experiments performed by Baker et al. [14]. Notably, the melts obtained experimentally have very low K_2O concentrations (less than 0.45 wt%, based on new analyses of the experimental glasses reported by Hirschmann et al. [27]). This is a key difference as K_2O has a major effect on melt compositions (see discussion in Section 5). They also display smaller compositional range and lower SiO_2 contents than the glass inclusions. These observations indicate that glass inclusions record an even smaller extent of melting than the diamond-aggregate experiments and also suggest a difference between the compositions of the starting materials.

Modelling the chemical trends recorded in the inclusions requires some knowledge about the mineralogical composition of the source. The primary mineral assemblage coexisting with the high-SiO_2 melts comprises olivine, orthopyroxene, spinel and as argued below clinopyroxene. Crystallization of clinopyroxene from the melt is indicated by its occurrence as interstitial neoblasts, but textural evidence such as the occurrence of ‘ghost’ clinopyroxene shows that primary clinopyroxene already existed in the nodule at depth. Residual clinopyrox-

ene is also indicated by increasing CaO contents with increasing MgO in glass inclusions, since it is the only CaO-bearing mineral in the peridotite assemblage. Given this information on the primary mineral phases of the peridotite source, one can calculate melt compositions produced for two different end-member melting processes: fractional melting where the produced melt is instantaneously extracted and batch melting where the melt remains in contact with the residual solid.

Na_2O versus K_2O and FeO versus MgO concentrations calculated for melt compositions during the two melting processes are shown in Fig. 3 (see caption of Fig. 3 for model parameters). K_2O is modelled as a highly incompatible trace element, with a constant bulk partition coefficient during the melting process [41,42]. In contrast, the Na_2O content of the melts is calculated using a non-modal melting model where Na_2O behaves as a moderately incompatible trace element mostly partitioned into clinopyroxene [43], with a decreasing bulk partition coefficient as clinopyroxene progressively melts out [15]. For deriving FeO and MgO concentrations of the melts, we used the approach of Langmuir and Hanson [44] and Langmuir et al. [15], where partition coefficients for FeO and MgO between olivine and liquid are parametrized as a function of temperature, pressure and liquid composition. We then used a Monte Carlo method for constraining the range of possible values for each model parameter (bulk partition coefficient, initial concentration in the source and proportion of clinopyroxene in the source) and their effects on the melt compositions. The best fits are obtained for a peridotitic source with a slightly depleted (0.20–0.23 wt%) Na_2O composition.

Changing the Na_2O concentration in the source to 0.30 wt% (typical values for fertile peridotite [45,46]) results in Na_2O contents that are too high

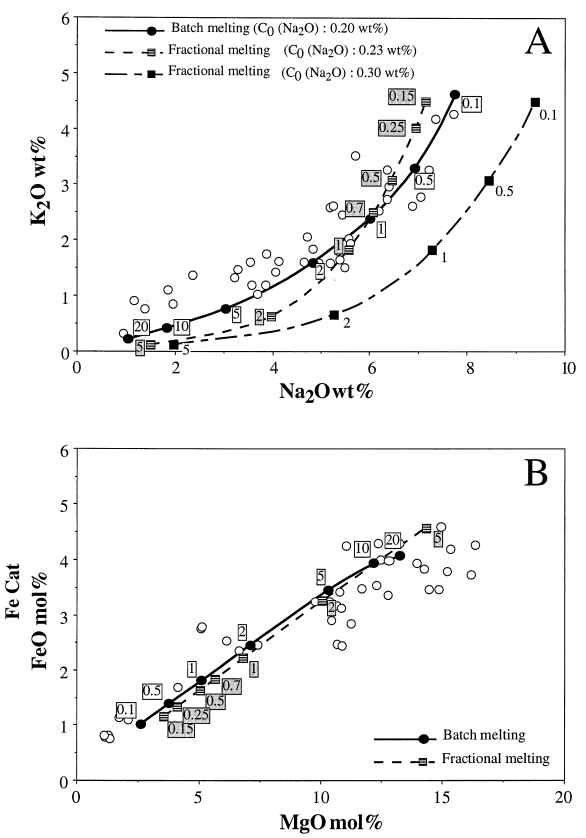

Fig. 3. (A) Plot of K_2O wt% against Na_2O wt% for rehomogenized glass inclusions, with various model curves showing calculated melt compositions produced by fractional and batch melting of peridotite. The curves are labelled with the extent of melting F (% melt). Note that for the fractional melting curve, instantaneous fractional melts are reported rather than the integrated average. The sodium contents of the melts is calculated using a non-modal melting model similar to Langmuir et al. [15], with D_{Na_2O} decreasing as clinopyroxene progressively melts out of the residue (cpx out for $F_{max} = 22\%$). The following parameters have been used. Fractional melting: melting trends have been calculated for a peridotite source with $Na_2O = 0.23$ and 0.30 wt%, $K_2O = 0.045$ wt%, a bulk partition coefficient for K_2O of 0.009, and a proportion of clinopyroxene in the source = 10% vol. Batch melting: melting trends have been calculated for a peridotite source with $Na_2O = 0.20$ wt%, $K_2O = 0.045$ wt%, a bulk partition coefficient for $K_2O = 0.009$, and a proportion of clinopyroxene in the source = 15% vol. (B) Plot of FeO against MgO in cation mole percent for rehomogenized glass inclusions, with melting curves produced by fractional and batch melting of peridotite, calculated using the method of Langmuir and Hanson [44]. The curves are labelled with the extent of melting F (% melt). The temperature and pressure dependence of the partition coefficient for MgO are taken from Langmuir et al. [15]. Melting trends have been calculated for a peridotite source with 6 mol% FeO and 56 mol% MgO. The other parameters are identical to those used in (A). The Si and Al contents of the melt composition used in the $K_D^{MgO/ol}$ parametrization are from corresponding glass inclusion data. The trends were calculated for a $K_D^{ol/liq} = 0.30 \pm 0.03$. Using lower $K_D^{ol/liq}$ values does not change the compositional range.

compared with the observed glass inclusion compositions. Conversely, the source concentration in K_2O obtained from the modelling is 0.045 wt%, while the K_2O content of mantle peridotite is considered to be about 0.03 wt% (e.g. [41,45]). A lower bulk partition coefficient for K_2O would decrease the K_2O concentration in the source, but it would also increase the curvature of the melting curves in the Na_2O versus K_2O diagram. Alternatively, the high K_2O concentration of the source may indicate an earlier metasomatic event, before the partial melting that produced the melts preserved inside inclusions. In order to explain the formation of extreme-composition interstitial glasses found in some xenoliths, Draper and Green [26] have suggested such pre-enrichment of the mantle in alkali oxides and volatile elements. Preexisting K_2O-bearing phase, especially phlogopite, is also often invoked as a potential source for K_2O-rich mantle melts (e.g. [23]). However, a strong limitation is the very low H_2O content of the silicic melts inside inclusions ($\leq$0.02 wt%, see Section 2), which precludes a significant amount of phlogopite (or amphibole) in the source, and therefore a significant effect on the K_2O budget. Assuming that all the water is contained in phlogopite and that $F \geq 0.2\%$, the maximum amount of phlogopite that could have preexisted in the mantle source is less than 0.05%.

The range in the extent of melting necessary to explain the data is much greater for batch melting (0.2–20%) than for fractional melting (0.2–5%). A purely batch melting process seems hardly reconcilable with the large differences in melt composition observed on scales of centimetres, and with the low maximum degree of melting expected for a relatively depleted peridotite source. On the other hand, the observation that, at the very small length-scale of the sample, melts are removed from grain boundaries where they have been generated and can be trapped along fractures within minerals without efficient pooling, supports the hypothesis that the cogenetic set of melt compositions recorded by the inclusions are formed by varying extents of fractional melting. A detailed discussion about melt distribution and simultaneous melting/deformation processes in peridotite, based on glass inclusion evidence, is given in Schiano and Bottinga [32]. A closer inspection of the Na_2O versus K_2O diagram shows that low-alkali glass inclusions plot slightly above the melting curves. This difference could reflect some mixing between different melt fractions, a process invoked by Plank and Langmuir [47] for MORB suites. The bulk partition coefficient for K_2O could also vary slightly as a function of the extent of melting. It should be noted, however, that the inferences drawn above are valid at the length scale of the xenolith and may or may not apply at the scale of mantle melting, some tens of kilometres. The mechanism of melt pooling at the length scale of the mantle could be greatly different.

An additional test for the melting model presented here is to consider the olivine/melt equilibration, in order to see whether the composition of the host CLG1 xenolith is consistent with the calculated residue of the melting process. We have thus calculated the residual olivine compositions in equilibrium with the calculated melts produced by fractional melting from 0.2 to 5% of a slightly depleted peridotite. The resulting compositions, when plotted in a FeO versus MgO diagram, compare favourably with the compositions of the olivine porphyroclasts in the CLG1 xenolith (Fig. 4). This in-

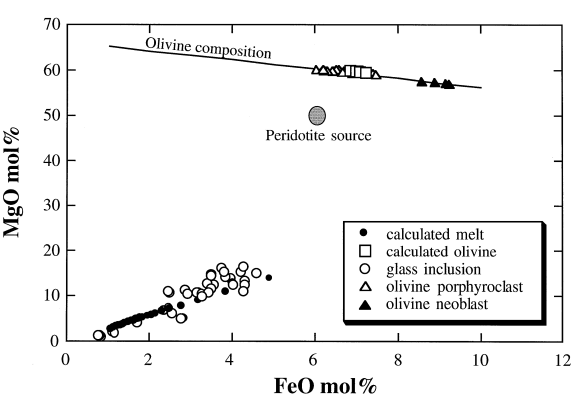

Fig. 4. MgO versus FeO diagram in cation mole percent, comparing the model compositions of the melts and residual olivine to the compositions of rehomogenized glass inclusions and olivine porphyroclasts in CLG1 xenolith. Parameters used for the fractional melting model are given in the caption of Fig. 2. Olivine neoblasts in the xenolith are added for comparison. The overlap between model olivine compositions and olivine porphyroclast data is in agreement with the hypothesis that the melts trapped in inclusions were derived from melting of a peridotite source similar to the CLG1 xenolith. The slightly larger range in FeO for the olivine porphyroclasts could reflect a variation in $K_D^{ol/liq}$ Fe–Mg as a function of the total alkali content of the melt as discussed in the text.

dicates that the olivine porphyroclasts are in equilibrium with the calculated melts, and therefore with the melts preserved inside inclusions. In contrast, olivine neoblasts ($Fo_{86–87}$) in the xenolith are markedly out of equilibrium (Fig. 4). Hence, our model calculations support the hypothesis of local equilibration between the high SiO_2 melts and their enclosing mineral phases.

5. Possible role for CO_2 during partial melting

On the basis of their high concentrations in incompatible elements, some alkaline oceanic lavas are considered to represent very low-degree melts (nephelinite, basanite). They are generally characterized by low SiO_2, high alkali oxides and FeO contents, in marked contrast with the near-solidus melts preserved as glass inclusions in peridotite minerals. This is illustrated by the clear offset between the compositions of inclusions in minerals from La Grille nodule and those of the host basanites in the FeO or SiO_2 versus MgO diagrams of Fig. 1. This apparent paradox can, at first sight, be related to the pressure of melting. At higher pressures, mantle melts have lower SiO_2 and higher FeO (and MgO) contents, even in a dry environment [5,48]. It might also reflect the role played by volatiles in the genesis of these different types of melts, in particular H_2O and CO_2, which have a major effect on the composition of silicate melts during partial melting (e.g. [49]).

Near-solidus diamond-aggregate experiments on peridotite performed by Baker et al. [14] were conducted with no or little volatile present, whereas CO_2 is the volatile species that dominates in glass inclusions. The evidence for CO_2 oversaturation of glass inclusions and the experimental data for CO_2 solubility in silicic melts [50] imply a CO_2 concentration in the trapped melt of around 0.45 wt%. In the presence of CO_2, melts are usually thought to be silica-poor rather than silica-rich (e.g. [51–53]). In contrast, phase diagrams for a peridotitic system indicate that the addition of H_2O shifts the composition of melts towards more silicic compositions [54]. However, FTIR spectroscopy measurements indicate very low water contents relative to carbon dioxide in high-SiO_2 glass inclusions. Hence, some other parameter has to be invoked to explain their high silica contents.

We suggest here that the reason why low-degree melts inside inclusions are silica-rich even though they are CO_2-saturated is linked (1) with the amount of CO_2 that can be dissolved in a melt as a function of pressure, and (2) with the speciation and interaction of CO_2 with cations within the melt.

At a pressure of 1 GPa, the solubility of CO_2 in silica-rich melts is low [55], and CO_2 is present mostly in the molecular form rather than as carbonate ions (CO_3^{2-}). At this pressure, the addition of Na_2O and, more efficiently, of K_2O in a silicate melt produces a decrease in the activity coefficient of SiO_2 ($\gamma_{SiO_2}^{liq}$), through the depolymerization of the SiO_2 network [53,56]. Therefore, if the melt coexists with ol + opx, a mineralogical assemblage buffering the SiO_2 activity ($a_{SiO_2}^{liq}$), this decrease in ($\gamma_{SiO_2}^{liq}$) is compensated by an increase in the SiO_2 content of the melt and, consequently, alkali and silica-rich melts are generated.

At higher pressures, the solubility of CO_2 and the concentration of CO_2 dissolved as carbonate (CO_3^{2-}) increase [57,58]. Moreover, the molecular CO_2/carbonate ratio decreases slightly [58] and the CO_3^{2-} ion appears as an efficient ligand, forming K_2CO_3, Na_2CO_3 and $CaCO_3$ complexes [59,60]. One may consider that, in this case, the alkali oxides do not have the potential to decrease significantly the activity coefficient of SiO_2, and therefore to increase the SiO_2 concentration of the melt.

In summary, we propose that the silicic compositions of the very low-degree melts formed at 1 GPa, and preserved as glass inclusions in CLG1 xenolith, result from a relatively low CO_2 solubility and a maximum effect of the alkali oxides on the silica activity coefficient. Based on experimental evidence, Hirschmann et al. [27] have also suggested that the effect of alkali oxides on the silica content of mantle melts decreases with increasing pressures, because of the decrease with pressure in the degree of polymerization for melts in equilibrium with mantle peridotite.

6. Conclusion

This study confirms that glass inclusions inside mantle minerals are remnant aliquots of partial mantle melts, and suggests that simultaneous

melting/deformation processes have major implications for melting in the upper mantle [32]. It further establishes that incipient melting of peridotite generates primary alkali and silica-rich melts, which may have SiO_2 contents up to 64 wt% for an extent of melting of 0.2%. It has been previously shown that silica-rich glass inclusions ubiquitously observed in mantle minerals from intraplate regions have a high potential as metasomatic agents [24]. This is demonstrated by their high contents in potassium and other incompatible elements. The results presented here suggest that these are simply very low-degree mantle melts, and that further melting of their sources produces melts more like erupted basalts. This genetic link between metasomatism and magmatism could reconcile two apparently contradictory observations [61], namely the evidence from xenolith studies for widespread metasomatism in the mantle, and the absence of extreme chemical heterogeneities recorded by basalts (e.g. [62]).

Acknowledgements

The authors are indebted to C. Langmuir and C. Farnetani for discussions that improved our understanding of the issues discussed in this paper. Thorough reviews by M. Hirschmann, F. Frey and R. Kinzler aided very much in revising the manuscript. E. Hauri provided a helpful review of an early version of the manuscript. M. Hirschmann generously shared a preprint, and made new analyses of glasses from the lherzolite-saturated experiments of Baker et al. [14] available to us. This is IPGP contribution number 1521. ***[CL]***

References

[1] K. Ito, G.C. Kennedy, Melting and phase relations in a natural peridotite to 40 kilobars, Am. J. Sci. 265 (1967) 519–538.
[2] D.H. Green, A.E. Ringwood, The genesis of basaltic magma, Contrib. Mineral. Petrol. 15 (1967) 103–190.
[3] I. Kushiro, Compositions of magmas formed by partial zone melting of the Earth's upper mantle, J. Geophys. Res. 73 (1968) 619–634.
[4] B.O. Mysen, I. Kushiro, Compositional variations of coexisting phases with degree of melting of peridotite in upper mantle, Am. Mineral. 62 (1977) 843–865.
[5] A.L. Jaques, D.H. Green, Anhydrous melting of peridotite at 0–15 kbar pressure and the genesis of the tholeiitic basalts, Contrib. Mineral. Petrol. 73 (1980) 287–310.
[6] E.A. Stolper, Phase diagram for mid-ocean ridge basalts: preliminary results and implications for petrogenesis, Contrib. Mineral. Petrol. 74 (1980) 13–27.
[7] E. Takahashi, I. Kushiro, Melting of a dry peridotite at high pressures and basalt magma genesis, Am. Mineral. 68 (1983) 859–879.
[8] T. Fujii, C.M. Scarfe, Composition of liquids coexisting with spinel lherzolite at 10 kbar and the genesis of MORBs, Contrib. Mineral. Petrol. 90 (1985) 18–28.
[9] E. Takahashi, Melting of a dry peridotite KLB-1 up to 14 GPa: implications on the origin of peridotitic upper mantle, J. Geophys. Res. 91 (1986) 9367–9382.
[10] T.J. Falloon, D.H. Green, Anhydrous partial melting of MORB pyrolite and other peridotite compositions at 10 kbar: implication for the origin of primitive MORB glasses, Mineral. Petrol. 37 (1987) 181–219.
[11] T.J. Falloon, D.H. Green, H.S.C. O'Neill, C.G. Ballhaus, Quest for low-degree mantle melts, Nature 381 (1996) 285.
[12] M.B. Baker, M.M. Hirschmann, L.E. Wasylenki, E.M. Stolper, M.S. Ghiorso, Reply to 'Quest for low-degree mantle melts', Nature 381 (1996) 286.
[13] T.J. Falloon, D.H. Green, H.S.C. O'Neill, W.O. Hibberson, Experimental test of low-degree peridotite partial melt compositions: implications for the nature of anhydrous near-solidus peridotite melts at 1 GPa, Earth Planet. Sci. Lett. 152 (1997) 149–162.
[14] M.B. Baker, M.M. Hirschmann, M.S. Ghiorso, E.M. Stolper, Compositions of near-solidus peridotite melts from experiments and thermodynamic calculations, Nature 375 (1995) 308–311.
[15] C.H. Langmuir, E.M. Klein, T. Plank, Petrological systematics of mid-ocean ridge basalts: Constraints on melt generation beneath ocean ridges, in: J. Phipps Morgan, D.K. Blackman, J.M. Sinton (Eds.), Mantle Flow and Melt Generation at Mid-Ocean Ridges, Am. Geophys. Union, Geophys. Monogr. 71 (1992) 183–280.
[16] R.J. Kinzler, T.L. Grove, Primary magmas of mid-ocean ridge basalts, 2: applications, J. Geophys. Res. 97 (1992) 6907–6926.
[17] T.J. Falloon, D.H. Green, C.J. Hatton, K.L. Harris, Anhydrous partial melting of a fertile and depleted peridotite from 2 to 30 kb and application to basalt petrogenesis, J. Petrol. 29 (1988) 1257–1282.
[18] R.J. Kinzler, C.H. Langmuir, Minute mantle melts, Nature 375 (1995) 274.
[19] D.H. Green, Composition of basaltic magmas as indicators of conditions of origin: application to oceanic volcanism, Philos. Trans. R. Soc. London A 268 (1971) 707–725.
[20] S.S. Sun, G.N. Hanson, Origin of Ross Island basanitoids and limitations upon the heterogeneity of mantle sources for alkali basalts nephelinites, Contrib. Mineral. Petrol. 52 (1975) 77–106.
[21] F.A. Frey, D.H. Green, S.D. Roy, Integrated models of basalt petrogenesis: a study of quartz tholeiites to olivine

melilitites from south eastern Australia utilizing geochemical and experimental petrological data, J. Petrol. 19 (1978) 463–513.
[22] E. Zinngrebe, S.F. Foley, Metasomatism in mantle xenoliths from Gees, West Eifel, Germany: evidence for the genesis of calc-alkaline glasses and metasomatic Ca-enrichment, Contrib. Mineral. Petrol. 122 (1995) 79–96.
[23] G.M. Yaxley, V. Kamenetsky, D.H. Green, T.J. Falloon, Glasses in mantle xenoliths from western Victoria, Australia, and their relevance to mantle processes, Earth Planet. Sci. Lett. 148 (1997) 433–446.
[24] P. Schiano, R. Clocchiatti, Worldwide occurrence of silica-rich melts in sub-continental and sub-oceanic mantle minerals, Nature 368 (1994) 621–624.
[25] P. Schiano, R. Clocchiatti, N. Shimizu, R.C. Maury, K.P. Jochum, A.W. Hofmann, Hydrous, silica-rich melts in the sub-arc mantle and their relationship with erupted arc lavas, Nature 377 (1995) 595–600.
[26] D.S. Draper, T.H. Green, P–T phase relations of silicic, alkaline, aluminous mantle-xenolith glasses under anhydrous and C–O–H fluid-saturated conditions, J. Petrol. 38 (1997) 1187–1225.
[27] M.M. Hirschmann, M.B. Baker, E.M. Stolper, The effect of alkalis on the silica content of mantle-derived melts, Geochim. Cosmochim. Acta, in press.
[28] E. Roedder, Fluid Inclusions, Rev. Mineral. 12 (1984), 644 pp.
[29] R. Clocchiatti, D. Massare, Experimental crystal growth in glass inclusions: the possibilities and limits of the method, Contrib. Mineral. Petrol. 89 (1985) 193–204.
[30] J.B. Lowenstern, Chlorine, fluid immiscibility, and degassing in peralkaline magmas from Pantelleria, Italy, Am. Mineral. 79 (1994) 353–370.
[31] A.V. Sobolev, V.L. Barkusov, V.N. Nevsorov, A.B. Slutsky, The formation conditions of the high-magnesian olivines from the monomineralic fraction of Luna 24 regolith, Proc. 11th Lunar Sci. Conf. 1980, pp. 105–116.
[32] P. Schiano, Y. Bottinga, Upper mantle partial melting as shown by fluid and melt/glass inclusions in ultramafic nodules from suboceanic hotspots, Geochim. Cosmochim. Acta, submitted.
[33] P.L. Roeder, R.F. Emslie, Olivine–liquid equilibrium, Contrib. Mineral. Petrol. 29 (1970) 275–289.
[34] R.J. Kinzler, T.L. Grove, Primary magmas of mid-ocean ridge basalts, 1: experiments and methods, J. Geophys. Res. 97 (1992) 6885–6906.
[35] R.J. Kinzler, Melting of mantle peridotite at pressures approaching the spinel to garnet transition: application to mid-ocean ridge basalt petrogenesis, J. Geophys. Res. 102 (1997) 853–874.
[36] M.F. Coffin, P.D. Rabinowitz, Evolution of the conjugate East African–Madagascar margins and western Somali Basin, Geol. Soc. Am., Spec. Pap. 226, 78 pp.
[37] T.L. Grove, R.J. Kinzler, W.B. Bryan, Fractionation of Mid-Ocean Ridge Basalt (MORB), in: J. Phipps Morgan, D.K. Blackman, J.M. Sinton (Eds.), Mantle Flow and Melt Generation at Mid-Ocean Ridges, Am. Geophys. Union, Geophys. Monogr. 71 (1992) 281–310.
[38] E. Wulff-Pedersen, E.-R. Neumann, B.B. Jensen, The upper mantle under La Palma, Canary Islands: formation of Si–K–Na-rich melt and its importance as a metasomatic agent, Contrib. Mineral. Petrol. 125 (1996) 113–139.
[39] P.B. Kelemen, H.J.B. Dick, J.E. Quick, Formation of harzburgite by pervasive melt–rock reaction in the upper mantle, Nature 358 (1992) 635–641.
[40] P.B. Kelemen, Reaction between ultramafic rock and fractionating basaltic magma, I: phase relations, the origin of calc-alkaline magma series, and the formation of discordant dunite, J. Petrol. 31 (1990) 51–98.
[41] A.W. Hofmann, Chemical differentiation of the Earth: the relationship between mantle, continental crust, and oceanic crust, Earth Planet. Sci. Lett. 90 (1988) 297–314.
[42] P. Schiano, C.J. Allègre, B. Dupré, E. Lewin, J.-L. Joron, Variability of trace elements in basaltic suites, Earth Planet. Sci. Lett. 119 (1993) 37–51.
[43] J.D. Blundy, T.J. Falloon, B.J. Wood, J.A. Dalton, Sodium partitioning between clinopyroxene and silicate melts, J. Geophys. Res. 100 (1995) 15501–15515.
[44] C.H. Langmuir, G.N. Hanson, An evaluation of major element heterogeneity in the mantle sources of basalts, Philos. Trans. R. Soc. London A 297 (1980) 383–407.
[45] E. Jagoutz et al., The abundances of major, minor and trace elements in the Earth's mantle as derived from primitive ultramafic nodules. Proc. 10th Lunar Planet. Sci. Conf. 1979, pp. 2031–2050.
[46] S.R. Hart, A. Zindler, In search of a bulk-Earth composition, Chem. Geol. 57 (1986) 247–267.
[47] T. Plank, C.H. Langmuir, Effects of the melting regime on the composition of the oceanic crust, J. Geophys. Res. 97 (1992) 19749–19770.
[48] K. Hirose, I. Kushiro, Partial melting of dry peridotites at high pressure: determination of compositions of melts segregated from peridotites using aggregates of diamonds, Earth Planet. Sci. Lett. 114 (1993) 477–489.
[49] P.J. Wyllie, Discussion of recent papers on carbonated peridotite, bearing on mantle metasomatism and magmatism, Earth Planet. Sci. Lett. 82 (1987) 391–397.
[50] J.R. Holloway, J.G. Blanck, Application of experimental results to C–O–H species in natural melts, Rev. Mineral. 30 (1994) 187–230.
[51] D.H. Eggler, Effect of CO_2 on the melting of peridotite, Carnegie Inst. Washington Yearb. 73 (1974) 215–224.
[52] W.L. Huang, P.J. Wyllie, Eutectic between wollastonite II and calcite contrasted with thermal barrier in MgO–SiO_2–CO_2 at 30 kilobars, with applications to kimberlite–carbonatite petrogenesis, Earth Planet. Sci. Lett. 24 (1974) 305–310.
[53] I. Kushiro, On the nature of silicate melt and its significance in magma genesis: regularities in the shift of liquidus boundaries involving olivine, pyroxene and silica minerals, Am. J. Sci. 275 (1975) 411–431.
[54] I. Kushiro, Effect of water on the composition of magmas formed at high pressures, J. Petrol. 13 (1972) 311–334.

[55] J.G. Blank, R.A. Brooker, Experimental studies of carbon dioxide in silicate melts: solubility, speciation, and stable carbon isotope behavior, Rev. Mineral. 30 (1994) 157–186.
[56] F.J. Ryerson, Oxide solution mechanisms in silicate melts: systematic variations in the activity coefficient of SiO_2, Geochim. Cosmochim. Acta 49 (1985) 637–649.
[57] J.G. Blank, R.A. Brooker, Experimental studies of carbon dioxide in silicate melts: solubility, speciation, and stable carbon isotope behavior, Rev. Mineral. 30 (1994) 157–186.
[58] E.M. Stolper, G.J. Fine, T. Johnson, S. Newman, The solubility of carbon dioxide in albitic melt, Am. Mineral. 72 (1987) 1071–1085.
[59] D.C. Rubie, W.D. Gunter, The role of speciation in alkaline igneous fluids during fenite metasomatism, Contrib. Mineral. Petrol. 82 (1983) 165–175.
[60] G. Fine, E. Stolper, The speciation of carbon dioxide in sodium aluminosilicate glasses, Contrib. Mineral. Petrol. 91 (1985) 105–121.
[61] A.W. Hofmann, Geochemistry and models of mantle circulation, Philos. Trans. R. Soc. London A 328 (1989) 425–439.
[62] A.W. Hofmann, K.P. Jochum, H.M. Seufert, W.M. White, Nb and Pb in oceanic basalts: new constraints on mantle evolution, Earth Planet. Sci. Lett. 79 (1986) 33–45.
[63] A. Späth, A.P. Le Roex, R.A. Duncan, The geochemistry of lavas from the Comores Archipelago, western Indian Ocean: petrogenesis and mantle source region characteristics, J. Petrol. 37 (1996) 961–991.
[64] C. Claude-Ivanaj, B. Bourdon, C.J. Allègre, Ra–Th–Sr isotope systematics in Grande Comore island: a case study of plume–lithosphere interaction, Earth Planet. Sci. Lett., in press.